CFD Analysis of Solar Air Heater Using V-Shaped Artificial Roughness to Attain Heat Transfer Enhancement

Abhishek Agarwal[1*] , Masengo Ilunga[2] , Karma Tempa[3] , Bharat Kumar Humagai[4]

[1] Department of Mechanical Engineering, College of Science & Technology, Royal University of Bhutan, Phuentsholing 21101, Bhutan
[2] Department of Civil Engineering, University of South Africa, Pretoria 1709, South Africa
[3] Civil Engineering Department, College of Science and Technology, Royal University of Bhutan, Phuentsholing 21101, Bhutan
[4] Department of Science and Humanities, College of Science and Technology, Royal University of Bhutan, Phuentsholing 21101, Bhutan

Corresponding Author Email: agarwala.cst@rub.edu.bt

ABSTRACT

The solar air heaters are generally used in food drying applications or air heating applications. The solar air heater encompasses the collector body, duct, absorber glass surface, air inlet, and air outlet tube. In the present research, the solar collector model is designed in Creo parametric design software and imported into ANSYS design modeler. The thermal analysis of the solar air dryer is conducted in the ANSYS CFX simulation package at different Reynolds numbers. To attain heat transfer enhancement, V-shaped artificial roughness is incorporated on the upper absorber plate. The V-shaped artificial roughness considered for the analysis are 60°, 90°, and 120° angles. From the thermal analysis, heat transfer coefficient (HTC) value, pressure drop, and thermos hydraulic performance parameter are determined for different V-shaped artificial roughness profiles. The CFD simulation results have shown that including ribs in the design of the solar collector enhances its heat transfer rate and THPF (thermos-hydraulic performance factor). The V-shaped ribs with a rib angle of 60° have shown superior thermal-hydraulic performance in comparison to rib angles of 90° and 120°, across all Reynolds numbers.

1. INTRODUCTION

The influx of Solar energy is the primary and predominant form of energy source on our planet. In the absence of an atmospheric layer, when the Sun is located at a distance of 1.495×10^{11} meters from Earth and has a diameter of 1.39×10^9 meters, its surface area perpendicular to its beams would generate an estimated power output of approximately 1353 watts. The planet receives solar energy at a rate of 170 trillion kilowatt-hours (kWh). Roughly 30% of the total energy is dissipated into the surrounding space through the process of reflection [1]. About 47% of the energy is transformed into low-temperature thermal energy. The Biosphere utilizes approximately 23% of the energy for the purposes of evaporation and precipitation. A small fraction, less than 0.5%, is captured and utilized through wind, wave action, and plant photosynthesis.

Solar energy systems consist of a collection of individual components. The solar air heater uses this solar energy for heating air which is then used for multiple purposes like food drying etc. [2]. The commercial design of the solar air heater is shown in Figure 1. The solar air radiators are responsible for facilitating the heat transfer between the absorber and the fluid in both directions, making them an essential component in these systems [3].

Figure 1. The general design of a solar air heater [4]

Typically, modifications are implemented on solar air purifiers with the objective of directly impacting their effectiveness. The increasing advancement of human

civilization has led to a greater reliance on natural resources to meet its essential needs. The dehydration of fruits and vegetables, such as grapes, pawpaw, and pepper, necessitates the utilization of fuel derived from natural resources through the process of combustion. Solar energy air radiators are a type of heat exchanger that transforms the thermal energy of the transport medium into solar radiation. Solar air heaters are essential components of solar systems. Solar air heaters, although they generate lower temperatures compared to other sun thermal air heaters, possess advantages such as a more straightforward design, reduced maintenance needs, and cost-efficiency. The advancement of solar air purifiers equipped with thermal storage technology has optimized the utilization of solar energy, resulting in enhanced efficiency and cost reduction.

Saini and Saini [5] conducted an experimental investigation on solar air heaters incorporated with arc-shaped roughness. The effect of geometric design parameters i.e. arc angle and e/D_h ratio is evaluated for HTC value and friction factor. The experimental analysis was conducted for Re number varying from 1200 to 17000. The experimental findings have shown an augmentation of Nusselt number (Nu) by nearly 3.8 times at an arc angle of 0.33 and d/D_h value of 0.042. The frictional factor is found to be minimal.

Saini and Verma [6] studied solar air collectors by changing geometric design parameters e/D_h and p/e (geometric designs). The thermal analysis was completed for an input number (temperature derivative ratio) varied between 1900 to 12400. The parameters for this analysis consist of a/b (0.018-0.037), and l/w (8-12) among other factors. Design parameters correlate in the following manner: Nusselt number and friction factor are found. The highest value, which is obtained for p/e = 10, is the one for which the friction factor is 0.0289. The experimentally validated computational fluid dynamics model used by Singh et al. [7] covers rib configurations of different geometries in down-flow systems. This work focuses on the effect of various rib geometries on thermal characteristics in S.A.Hs. This study also shows that a half-trapezoidal rib design offers the maximum enhancement in thermal efficiency and that the efficiency is 17% higher. Quarter circulars also do well and offer thermal performance enhancement of 16 percent in this case. Apart from the thermal analysis, the paper presents useful insights in relation to the frictional losses. Concerning the static pressure distribution, it was pointed out that all the quarter-circular rib types analyzed reveal about 10% lower friction than trapezoidal ribs, which was seen as a proper compromise between thermal enhancement and flow resistance.

Furthermore, the study also focuses on exergy recovery to measure the efficiency of the mentioned rib designs. The investigation on trapezoidal and circular ribs PAHs reveals that the ribbed surface enhances the exergy entity by 35% compared with a flat smooth SAH. This important result shows that these configurations of ribs can improve the efficiency of the entire system. Thianpong et al. [8] conducted experimental investigations on solar air heaters by incorporating isosceles triangular ribs. The arrangement of ribs is done in staggered type and in-plane type for Re values ranging from 5500 to 22000. The analysis is conducted with varying hydraulic diameters to pipe diameters varying between 0.0733 and 0.147. The analysis is conducted for both symmetric and asymmetric rib configurations. From the analysis, it was found that in-line rib design has shown a higher Nusselt number and friction factor as compared to

staggered design configuration. The maximum thermal performance of SAH is observed for an e/D_h value of 0.145.

Kazemi Moghadam et al. [9] have investigated a solar air heater having arc-shaped ribs newly designed to investigate the thermal performance of the augmenter by numerical analysis. The heat transfer characteristics of the augmenter are investigated comprehensively. For Reynolds numbers 6000 and 12000, the effects of different design factors involving cross-sectional shapes, spacing, aspect ratio, and rib pitch on thermal performance are investigated. The tests suggest that the quadrangular-shaped ribs provide the greatest coefficient of performance when compared to other shapes. Moreover, the study reveals that when the rib pitch is set to 40 mm and the aspect ratio to 0.5, thermal performance is improved. In particular, it became possible to establish that the spacings between the ribs influenced the solar air heater's thermal efficiency to the least extent. These correlations are expected to help in the better design and better performance of the solar air heaters in practical application. Kumar et al. [10] performed an investigation of SAH by incorporating W-shaped ribs on an absorber plate. The thermal energy was selectively transferred to the absorber plate, while the remaining surfaces were maintained at adiabatic conditions. The rectangular duct was measured to have an aspect ratio of 8:1. The analysis was conducted for Re value ranging from 2800 to 15000, for e/D_h value ranging from .0168 to .0338, and AOA varying from 30° to 75°. The maximum heat transfer enhancement is attained for an e/D_h value of 0.035.

Chompookham et al. [11] steered an experimental investigation on the rectangular duct of SAH. The channel geometry has a P/H ratio of 1.33, e/H ratio of 0.2. The analysis was conducted to determine the thermal characteristics of the fully developed turbulent fluid. The thermal boundary conditions are applied on the upper face of the duct and on the absorber surface. The subsequent analysis was conducted by incorporating WVG vortex generators at the inlet zone of the duct. The application of WVG vortex generators has shown a 5.8% enhancement of HTC value at an AOA value of 60°.

The efficacy of a two-phase integrated absorption cooler was investigated by Farhan [12] by combining experimental and theoretical approaches. The proof of DPSAH by Metrologic hour data collected through December 2016 and January 2017 was specifically for the Baghdad region in Iraq. The research showed that the air equivalent factor of the framework surged when the airflow velocity increased through the collector. This caused a rapid decrease in the temperature of the air leaving the system. It, further, helps with the primary output of electricity and improves the recovery use to be more efficient as well. At 12 PM, the temperature and speed reading on the air outlet were approximately 3 App degrees and a flow rate of 0.01 cubic meters per second respectively. The degree of value for the Swirl-Trapping researchers was increased by 6% when the DPSAH design was used in the place of single pass design configuration (SPSAH) at constant airflow velocity.

Momin et al. [13] conducted an experimental investigation of SAH incorporated with V-shaped ribs. The V-shaped ribs are placed at the bottom of SAH and the Re number is varied from 2500 to 18500, with e/D_h value ranging from 0.02 to 0.034, and AOA value ranging from 30° to 90°. The increase of friction factor and HTC values are determined and the effect of e/D_h on friction factor, HTC is established and compared with roughened surface.

Matheswaran et al. [14] conducted thermal analysis on

double-pass SAH using numerical techniques. The energy and exergy analysis are conducted for SAH with varying artificial roughness. The numerical results obtained are validated with the experimental test results available in the literature. The results of exergy and energy analysis obtained from double-pass SAH are compared with the results obtained from single-pass SAH. The results have shown that double-pass SAH has better performance as compared to single-pass SAH by 8% (exergy analysis) and 7.1% (energy analysis).

Matheswaran et al. [15] conducted experimental testing on single pas SAH mass flow rate ranging from 0.002 to 0.023 Kg/s. The energy and exergy analysis are conducted for different pitch ratios ranging from 0.435 to 0.869. The research findings have shown that exergy efficiency increases by 21.2% by varying pitch ratios and energy efficiency increases by 22.4%. The exergy efficiency is found to be affected by different parameters i.e. mass flow rate, X/D_h, and Y/D_h ratios. The optimal performance is attained at (X/D_h = 1.739), the span-wise pitch ratio (Y/D_h = 0.869), diameter ratio (D_j/D_h = 0.065), and mass flow rate of 0.0035 Kg/s. The correlations between Re number and jet plate design variables are established. Panda and Kumar [16] analyze the use of artificial roughness on the surface of the solar air heaters expose to heat to increase the heat transfer rate of the fluid through the air duct. The study also points out that artificial roughness is an effective mechanism when it comes to enhancing thermal performance. The authors explore different roughness geometries and their effect on both heat transfer and friction in the solar air heater studied. His review focuses on the factors that various geometries of the elements applied as artificial roughness must have to enhance the thermal and thermo-hydraulic characteristics of the solar air heater ducts. Much can be learned from this work, especially the best strategies to employ in the design of solar thermal systems towards energy efficiency. Saxena et al. [17] presented various types of roughness geometries in detail to increase the SAH efficiency with artificial roughness. The study presents a systematic comparison between various rib shapes as well as their heat transfer coefficients. Therefore, this study finds that using different types of rib forms in the SAHs can offer great potential benefits related to optimized thermal enhancement, which is highly informative for various design strategies applied in solar thermal systems. Kumar et al. [18] compared the results of an experimental investigation carried out for the efficiency of absorber plates with and without rib roughness. Both configurations are black painted with dispersed graphene nanoparticles into the paint. The researchers used a numerical and experimental approach to evaluate how surface roughness affects friction factors and heat transfer characteristics. The findings also suggest that smooth plates are on average up to 12% more efficient at converting heat into useful work than rough plates, with overall efficiencies of 4.82 and 4.46 respectively. This research therefore establishes that surface characteristics play a crucial role in the utilization of solar thermal systems. Esmaeili Shayan et al. [19] investigated the performance impact of different geometrical positions of the rectangular S-shaped artificial roughness placed inline and staggered in solar air heaters. This research proposes to validate the improvement realized in thermo-hydraulic performance utilizing different roughness configurations. Such characteristics as the length and height of the roughness elements, and the constant size of intervals between them fall under key parameters considered. The Reynolds number was set from 3,000 to 10,000 and the pitch was changed for the

inline positions, while the length ratios were changed for the staggered ones. The maximal values of the Nusselt number, which characterizes heat transfer intensity, were noted at the given pitch-to-height ratio for both cases, and they were 4.87 and 4.2 times higher than those for a smooth tube.

The technological potential of solar air heaters (SAH) has been explored in numerous studies. However, there is no comprehensive understanding of the impact of rib angles on the thermal-hydraulic performance of the SAH. So far, research has been mainly oriented to the effect of rib shapes and configurations on heat transport and the characteristics of fluid flow. Nevertheless, the exact role of rib angles, mainly V-shaped, on the general behavior of these structures is still largely unknown. This is the aspect that needs to be kept in mind for designing and enhancing the SAH efficiency, especially its thermal-hydraulic performance. For this study, it is hypothesized that changing the angles of V-shaped ribs on the solar-air-heater will play a noteworthy part in the thermal-hydraulic efficiency of the system. Particularly, it is predicted that various rib angles would produce differing amounts of heat transfer improvements and friction factors, which necessarily affect the overall THPF of the solar air heater. The Research Questions considered in this study are:

1. The role of varying rib angles in V-shaped ribs in the heat transfer properties of a solar air heater:

2. How does the angle of the rib affect the friction factor in a solar air heater?

3. How do the different rib angles contribute to the thermal-hydraulic performance factor (THPF) of a solar air heater?

4. What is the best possible value of the rib angle that maximizes the thermal-hydraulic performance of the solar air heater?

The objective of the present study is to perform CFD simulation using ANSYS CFX software by varying rib angles. The roughness profile used for analysis is V-shaped with varying rib angles and keeping the depth constant for all analyses whereas roughness angles are varied from 60°, 90°, and 120°. Nusselt number and friction factor are calculated at various Reynolds numbers. Using these two parameters THPF is computed.

2. METHODOLOGY

An analysis is conducted on a rectangular segment as shown in Figure 2. The dimensions of the test length are 280 mm, the entry length is 245 mm, and the exit length of 115 [20]. The hydraulic diameter of the duct is 0.033 m.
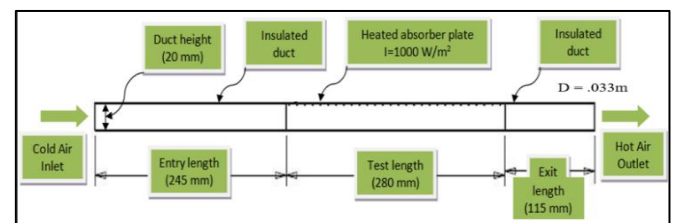

Figure 2. Sketch of the computational domain

2.1 CAD modelling

The CAD model of V-shaped ribs, as seen in Figure 3, is created using Creo parametric design software. The CAD model is developed using a sketch tool, followed by extrusion,

a V-shaped extrusion cut. The multiple copies of the V-shaped cut are generated using the pattern tool as shown in Figure 3.
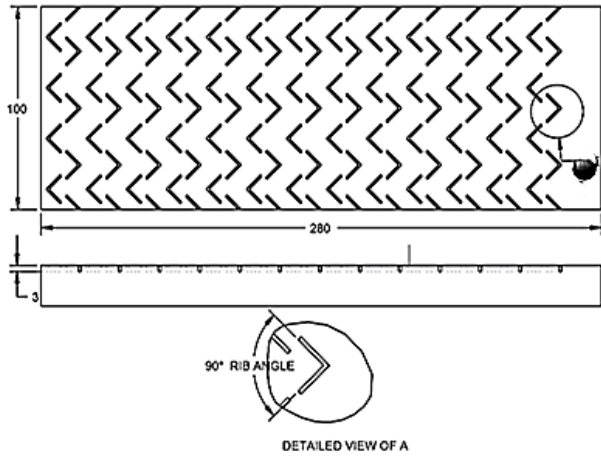

Figure 3. V-shaped ribs with 90° rib angle

The depth of rib is 0.006 m and slant length of rib is 0.01 m whereas the thickness of rib is 0.001 m as shown in Figure 4 and Figure 5 respectively. The Creo parametric software has sketch tool on which sketch of V-shaped ribs is developed. The sketched model of V-shaped ribs is extruded up to specific depth of 6 mm.
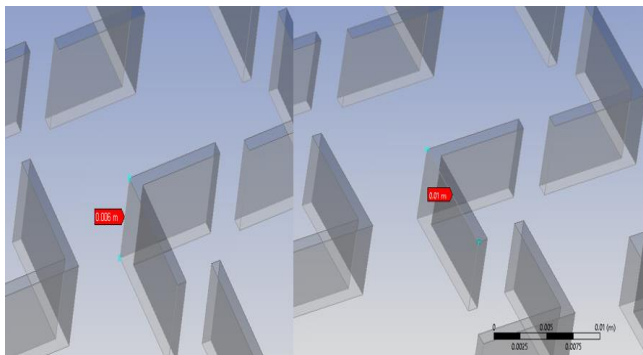

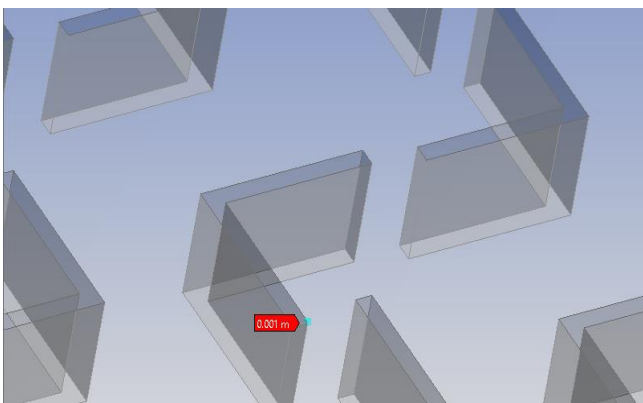**Figure 4.** Height and edge length of V-shape ribs

Figure 5. Thickness of rib

The extrude type used is "cut" which removes material. After modeling of single rib, multiple ribs are generated using pattern tool. Likewise, multiple rows of ribs are generated using pattern tool. The CAD model developed as per the schematic shown above is shown in Figure 6 below.
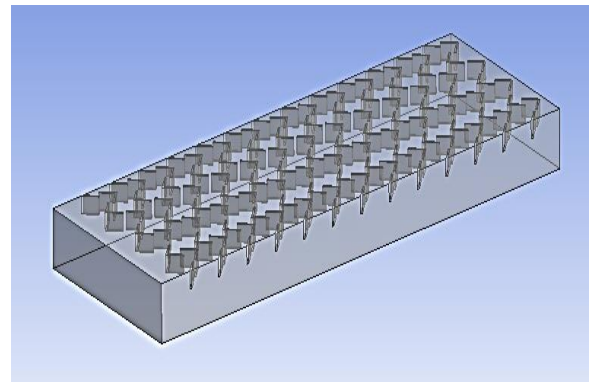

Figure 6. CAD model of smooth plate

2.2 Meshing

The CAD model created in Creo is converted to the .iges file and loaded into ANSYS. In ANSYS, the model is then meshed and subjected to loads and boundary conditions [21]. The model is discretized using tetrahedral components, with the inflation set to the typical level, as seen in Figure 7.
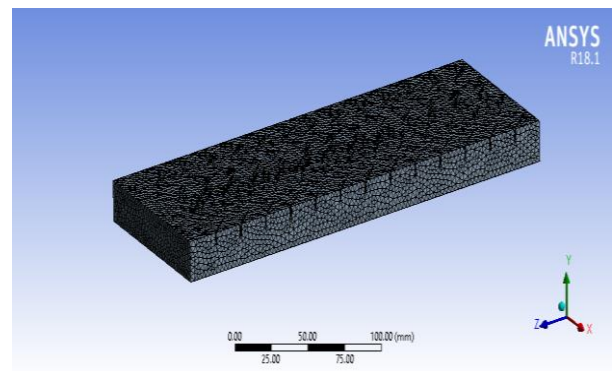

Figure 7. Meshed model of smooth plate

The CFD preferred tetrahedral elements since they are capable of representing complex geometries with high accuracy and efficiency. These meshes are flexible enough to fit curvatures well, can be adjusted in certain regions, and comply with ANSYS CFX and other major CFD solvers, which makes them a good option for simulations.

2.3 Domain definition: loads and boundary

After meshing the model is applied with appropriate loads and boundary conditions in the setup module of ANSYS CFX as shown in Figure 8.
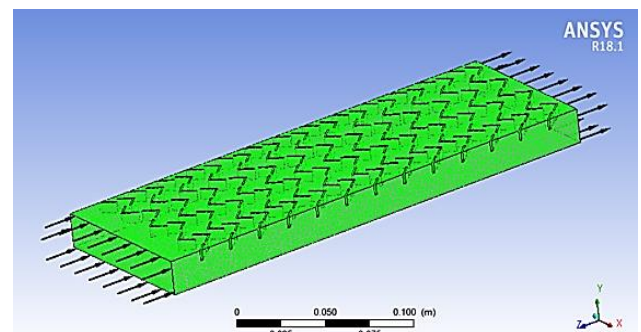

Figure 8. Loads and boundary conditions

174

The process involves domain definition. In the process, the domain type is set to fluid type, the energy model is set to thermal energy type with a reference pressure of 1atm. The domain is defined with fluid as air, and the energy model is set to thermal energy and the turbulence model is set to k-epsilon [21]. The reference pressure is set to 1 atm, with morphology as a continuous fluid. The physical properties of the air used are shown in Table 1 below.

Table 1. Thermo-physical properties of aluminum and air [20]

Properties	Working Fluid (Air)	Absorber Plate (Aluminum)
Density, ρ (kg/m^3)	1.225	2719
Specific heat, C_p (J/kg k^{-1})	1006.43	871
Viscosity, μ (N/m^2)	1.7894×10^{-5}	-
Thermal conductivity, k (W/m k)	0.0242	202.4
Prandtl number, Pr	0.7441	-

The inlet/outlet and wall boundary conditions are defined. The inlet velocity and turbulence are described in the next section as shown in Table 2.

Table 2. Reynolds number and velocity

Reynolds Number	Inlet Velocity (m/sec)
3900	1.67
5500	2.20
8500	3.51
12500	5.26
15500	6.58
18500	7.89

The assumptions are:

1. The duct walls were assumed to be isotropic and homogenous.

2. Steady, turbulent, and fully developed two-dimensional-flow.

3. The absorber plate and the duct wall thermal conductivity were temperature-independent.

4. Negligible heat losses and no radiation heat transfer.

5. At the junction of wall and fluid, no-slip boundary conditions were assumed.

6. The absorber plate and working fluid (air) properties were invariable at an average bulk temperature of 300 K.

During the initial stage, ANSYS incorporates and calculates the recommended turbulence intensity using the formula.

$$I = 0.16 \times Re^{-1/8} \tag{1}$$

Boundary conditions were set at the outflow with a constant pressure of 101300 Pascal (Pa).

All remaining edges were classified as walls with insulated borders. The K-epsilon turbulence model is employed for the purpose of analysis. A uniform heat flux of 1000 W/m^2 is applied to the upper surface [21].

3. RESULTS AND DISCUSSION

The way that section titles and other headings are displayed in these instructions, is meant to be followed in your paper. Validation and Grid Independence: for validation, the CFD analysis is conducted on the solar air heater having smooth duct i.e. without any artificial roughness. Selection of the best grid size is very important to achieve accurate results. Hence, grid independence tests were performed to predict appropriate grid dimensions to carry out the numerical simulations over a range of Reynolds numbers. The grid independence test was conducted at Re = 3800. In the grid independence test, the total number of grids was increased till the difference in results between two consecutive grid sizes became negligible. At this moment, the grid size corresponding to the second last case of the grid independence test was considered to be the best one and it was used for further simulations. The temperature distribution plot is shown in Figure 9.
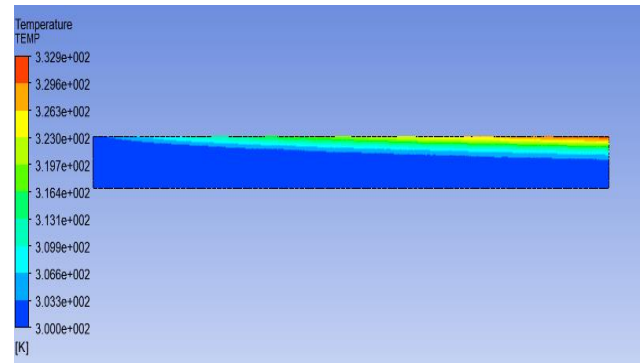

Figure 9. Temperature distribution plot

Separate grid independence tests were conducted for different geometries. From the grid independence table (Table 3) the results of mean temperature remain concurrent and therefore for our analysis, we have selected 79685 number of elements.

Table 3. Grid independence evaluation

Number of Elements	Average Mean Temperature (K)
78895	303.9
78985	303.85
79289	304.01
79548	304.12
79685	304.12

Table 4 shows the percentage deviation in Nusselt number for smooth duct between Dittus-Boelter correlation results and CFD results and the graphic representation is shown in Figure 10.

Table 4. Percentage deviation in Nusselt number for smooth duct between Dittus-Boelter correlation results and CFD results

#	Reynolds Number	Nus from Dittus-Boelter Correlation	Nus from CFD Results	Error (%)
1	3800	14.32	14.93	-4.118%
2	5000	18.235	18.59	-1.962%
3	8000	28.135	27.09	3.8192%
4	12000	38.185	37.46	1.9082%
5	15000	44.63	44.69	-0.357%
6	18000	50.28	51.84	-2.991%

The maximum deviation in Nusselt number (Nu) is 4.119% which shows a good agreement between the correlations and CFD values ensuring the accuracy of the analysis. After conducting CFD analysis on ANSYS CFX the contour plots of

pressure, temperature, and turbulence kinetic energy are plotted. In the next stage, CFD simulation is carried out on rectangular ducts with varying rib angles. The depth is kept constant at 3 mm, and rib angles are varied from 600, 900, and 1200. Nusselt number, friction factor is determined which is used to calculate THPF.
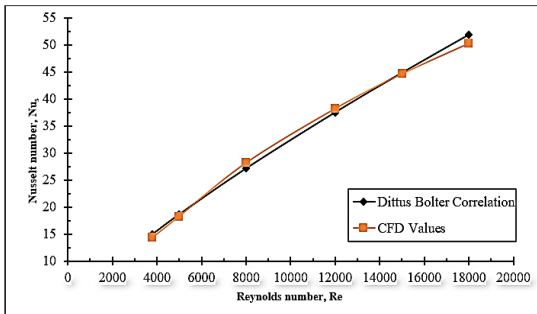

Figure 10. Nusselt number VS. Reynolds number

3.1 Case 1: CFD analysis with 600 rib angles

The temperature plot, as shown in Figure 11, produced with a roughness height of 3 mm and an angle of 600 at a Reynolds number of 3900 exhibited non-uniform temperature change over the length of the duct. The maximum temperature is 318 Kelvin, while the minimum temperature is 300 Kelvin.
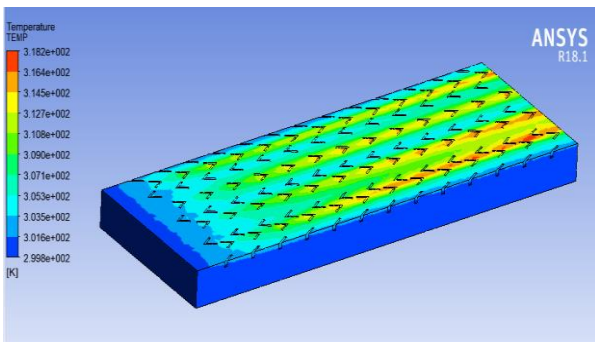

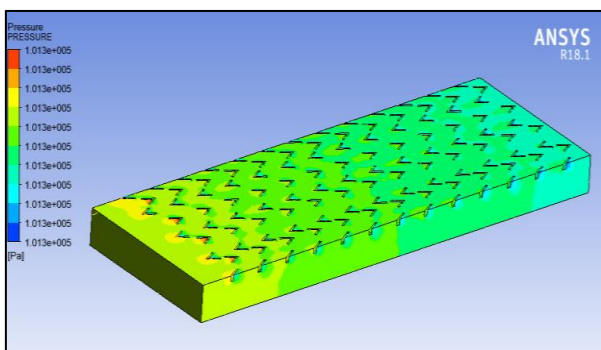**Figure 11.** Temperature plot at 3900 Reynolds number

Figure 12. Pressure plot at 3900 Reynolds number

The pressure at the intake is initially greater and gradually decreases as it progresses towards the outlet, as seen in Figure 12. The pressure is elevated in the intercostal spaces directed toward the intake face, as shown by the red coloration.
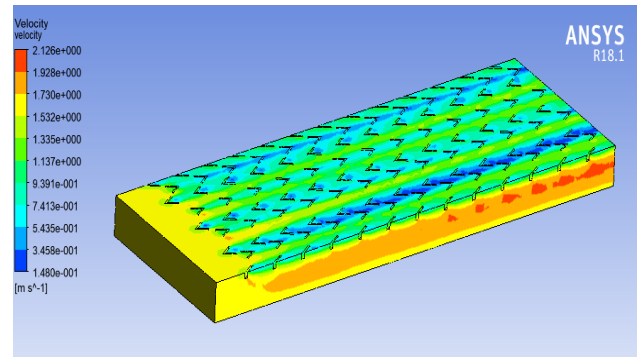

Figure 13. Velocity plot at 3900 Reynolds number

The velocity plot shown in Figure 13 illustrates a decrease in velocity between ribs, as seen by the light blue and dark blue colors along the rib row. The highest velocity achieved is located at the outlet area, shown by the dark red hue. The velocity disparity between the absorber face and rib face at the bottom results in the formation of vortices. Turbulent flow enhances the rate of heat transfer. The greatest velocity achieved is 2.12 m/s, while the smallest velocity achieved is 0.14 m/s.

3.2 Case 2: CFD analysis with 900 rib angles

The plot in Figure 14 displays the results obtained with a roughness height of 3 mm, specifically at a rib angle of 900. Below are the temperature plot, pressure plot, and velocity plot.
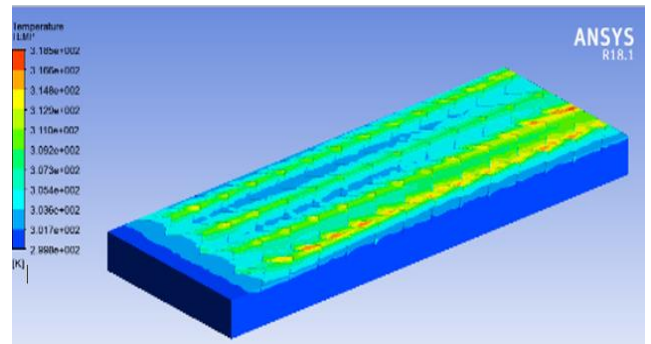

Figure 14. Temperature plot at 3900 Reynolds number

The temperature plot shows an uneven distribution of temperature over the length of the duct. The temperature gradient is seen to be higher in the vicinity of the ribs, as shown by the green contours, and decreases as we approach farther away from the ribs, as indicated by the light blue contours. The temperature exhibits variation in both the horizontal and vertical directions. The maximum temperature is 318K and the minimum temperature is 300K.

The pressure plot indicates the formation of a high-pressure region at the entrance section, with a non-uniform decrease in pressure as we go towards the duct outlet, as seen in Figure 15 below.

The air velocity experiences a significant decrease in proximity to the rough surface, but it gradually increases as we go farther away from it. This trend is visually represented by the light green and yellow colors in Figure 16.
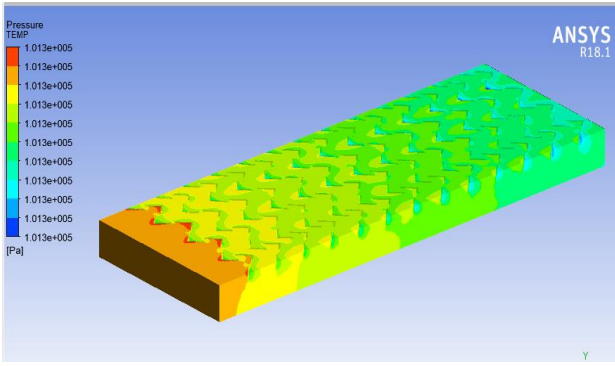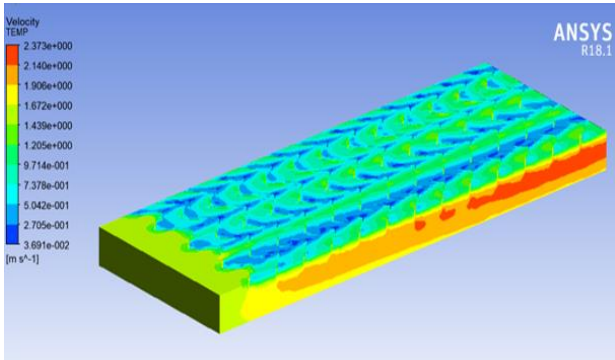
Figure 15. Pressure plot at 3900 Reynolds number

Figure 16. Velocity plot at 3900 Reynolds number

3.3 Case 3: CFD analysis with 1200 rib angles

In this section results obtained from a roughness height of 3 mm are plotted at 1200 rib angle. The temperature plot, pressure plot, and velocity plot are given in Figure 17.

Figure 17. Temperature plot at 3900 Reynolds number

The temperature plot as shown in Figure 17 obtained for roughness height 3 mm and 1200 angle at 5500 Reynolds number shown a non-uniform variation of temperature across length of the duct. The highest temperature is 325K and the lowest is 300K. The maximum temperature is seen near the rib end position.

The pressure at the inlet is higher and reduces as it moves towards the exit as shown in Figure 18. The pressure is higher in between the ribs facing towards the inlet face as shown by the red color.

The velocity plot shown in Figure 19 below shows a reduction in velocity between ribs and near to rib row shown by light blue and dark blue color. The maximum velocity attained is near the outlet section shown by dark red color. The

velocity difference between the absorber face and rib face at the bottom causes' vortex generation. The vortex or turbulent flow increases the heat transfer rate. The maximum velocity attained is 2.45 m/s and the minimum velocity attained is .012 m/s. The difference between maximum and minimum velocity is higher across the length of the duct thereby creating a higher pressure drop. Table 5 shows that the Nusselt number increases with an increase in the Reynolds number for all angles of ribs.
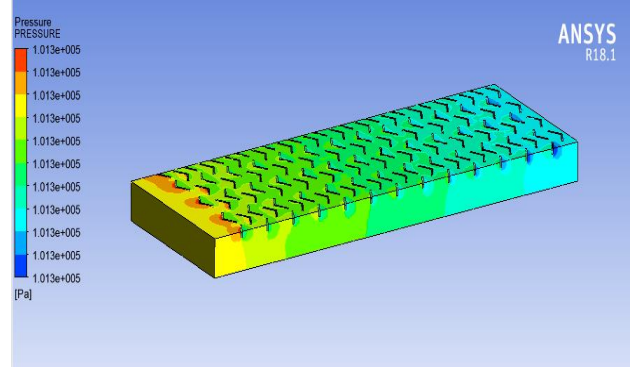

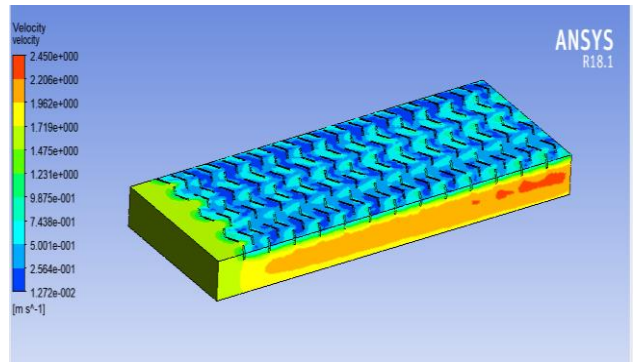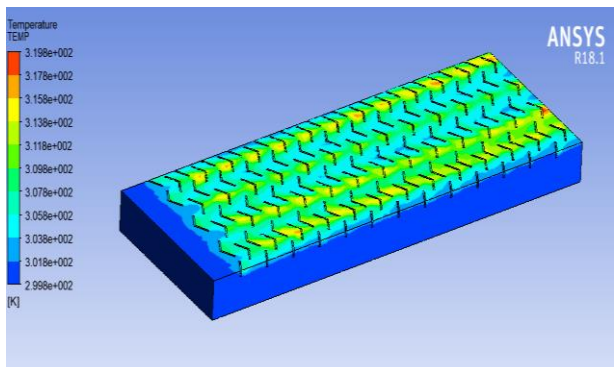**Figure 18.** Pressure plot at 3900 Reynolds number

Figure 19. Velocity plot at 3900 Reynolds number

Table 5. Nusselt number of different angle ribs

Reynolds Number	3900	5500	8500	12500	15500	18500
Smooth	14.92	18.5	27.2	37.46	44.78	51.82
600	28.71	40.2	69.7	104.84	127.77	148.31
900	32.81	45.04	75.59	111.14	134.07	154.73
1200	33.32	45.64	75.21	108.55	129.7	149.04

Figure 20 shows that Nusselt number increases with increase in Reynolds number for all angles of ribs.

At low Reynolds number i.e. 3900 and 5500, 120° rib angle and 90° rib angle has almost same value and for higher Reynolds number 90° rib angle exhibited higher Nusselt number.

At low Reynolds numbers i.e. 3900 and 5500, 120° rib angle and 90° rib angle have almost the same value, and for higher Reynolds numbers 90° rib angle exhibited a higher Nusselt number. The friction factor is calculated using the pressure difference obtained from the CFD solution and tabulated in Table 6.

Friction factor generally decreases with increase in Reynolds number as can be seen in Figure 21. At 60° rib angle friction factor first increases then decreases with increase in Reynolds number. At 120° rib angle friction factor decreases after 8500 Reynolds number.
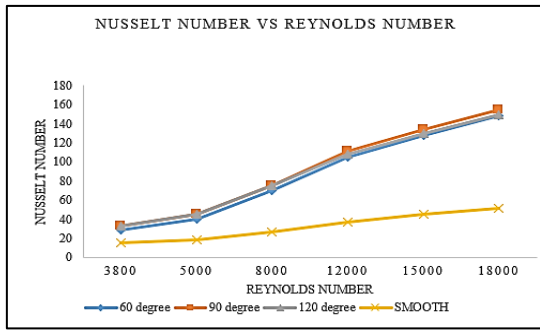
Figure 20. Nusselt number VS. Reynolds number

Table 6. Friction factor at different rib angles

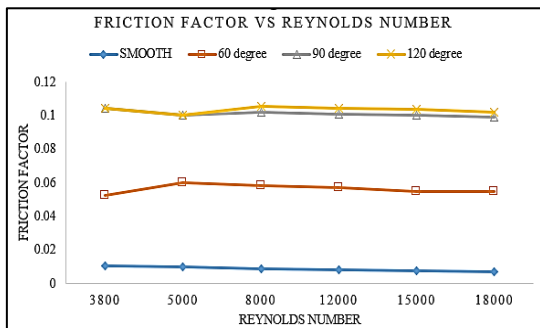| Reynolds Number	3900	5500	8500	12500	15500	18500
SMOOTH	0.01082	0.00988	0.00869	0.00799	0.00765	0.00732
600	0.0522	0.06	0.058	0.057	0.055	0.055
900	0.1045	0.10008	0.1018	0.101	0.10008	0.0989
1200	0.1045	0.10008	0.1057	0.1044	0.1034	0.102

Figure 21. Friction factor VS. Reynolds number

The friction factor generally decreases with an increase in Reynolds numbers. At a 60° rib angle friction factor first increases and then decreases with an increase in Reynolds number. At a 120° rib angle friction factor decreases after 8500 Reynolds number. THPF is calculated using the ratio of Nusselt number and friction factor which is tabulated in Table 7.

Table 7. THPF at different rib angles

Reynolds Number	3900	5500	8500	12500	15500	18500
600	1.15	1.19	1.403	1.448	1.475	1.45
900	1.031	1.115	1.289	1.28	1.278	1.253
1200	1.046	1.138	1.209	1.224	1.213	1.197

The THPF value is found to be highest for 600 rib angles with the maximum value of 1.47 at 15500 Reynolds number. A minimum THPF value is observed for 900 rib angles at 3900 Reynolds number with a value of 1.033. In the aspect of higher Reynolds numbers, 1200 rib angles have consistently ensured the lowest THPF compared to the other two rib angles. THPF VS. Reynolds number is shown in Figure 22.

As its evident from Figure 22 THPF value is found to be highest for 600 rib angles with maximum value of 1.47 at 15500 Reynolds number. Minimum THPF value is observed for 900 rib angles at 3900 Reynolds number with value of 1.033. For higher Reynolds number 1200 rib angles has shown lowest THPF values compared to other two rib angles.
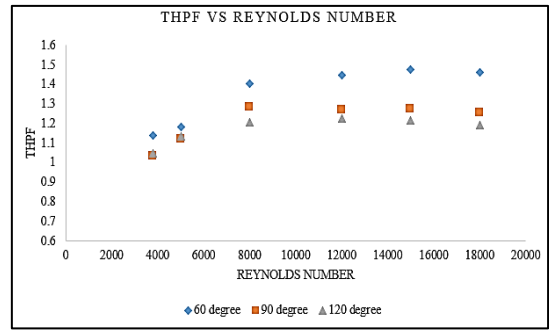

Figure 22. THPF VS. Reynolds number

4. CONCLUSIONS

The comprehensive study reveals the outcome of a numerical analysis of airflow and heat transfer inside the duct in a solar air collector. On the absorber side, there are man-made V-shaped ribs, which are angled. The research was carried out with the help of numerical software that was based on CFD methods. The CFD simulation was used to determine the impact of absorber roughness on airflow and the enhancement of heat transfer in solar air heaters. It was found that the inclusion of the ribs in the design of the solar collector contributed to its convective heat transfer factor and thermos-hydraulic performance. V ribs with the rib angle of 60° have shown superior thermal-hydraulic performance compared to the other rib angles of 90° and 120° at all Reynolds numbers. The research hypothesis, which was concerned with how changing rib angles would affect the air-water (thermal-hydraulic performance) of solar devices, supported the results. The research questions about the effect of rib angles on heat transfer rate and THPF were answered by the CFD simulations.

To improve the effect of generating more vortices, the angle between the ribs is at 60° thus providing better and more consistent shapes of the ribs. These vortices help in increasing the level of turbulence in the fluid and disturbing the thermal boundary layer in a better way. This disruption also results to a higher value of heat transfer coefficient of convection thus high values of Nusselt numbers. Through the interaction of the 60° ribs, flow instabilities encouraging strong secondary flow are created to improve the transfer of heat away from the heated surface. Such flows help in getting a better temperature gradient and higher heat transfer coefficients. In a similar way, the increase in the angle of the ribs used in hollow plates conventionally improves turbulence and also raises the pressure drop. The 60° angle offers the best compromise where there is a higher improvement in turbulence (and thus heat transfer) while the pressure drop is not excessively high. This in turn leads to a higher value for the Thermo-Hydraulic Performance Factor (THPF). The main outcome points are:

1. Angle ribs of 60° make strong vortices and turbulence in the flow field because of its geometry. These vortices tend to pull or rotate and break up that thin layer of fluid around the absorber plate so as to enhance the interaction between the fluid and the plate for heat exchange. The flow disturbance near the surface is higher for the present configuration, which improves heat transfer by convection leading to higher Nusselt number as compared to smooth surfaces and or ribs in various orientations.

2. It allows for the ribs' 60° angle that helps to create the controlled separation and reattachment of the flow further along the surface of the plate. These are abnormal slopes,

which play a part in detaching and reattaching boundary layers and seem to have an effect on heat transfer. Proper timing to reestablish the flow with lower energy, minimize the growth of the flow's boundary layer, and thus minimize thermal conduction and maximize heat exchange.

3. The 60° ribs demonstrate the best height and angle for cutting the thermal boundary layer properly. This disruption enhances the capability of flowing air to transfer heat with better enhancement of thermal penetration over the surface of the entire duct. Higher values of thermal penetration increase the effect of convection, or the heat transfer coefficient, thus thinning the thermal boundary layer and Nusselt numbers.

4. Although the 60° ribs improve the heat transfer rates, they also increase the pressure drop due to the increased frictional resistance offered by the ribs to the flow. Thus, heat transfer rates increase while pressure drop increases resulting to an improvement in the thermal-hydraulics of the system. The promoters of the Nusselt numbers in the case of the 60°ribs again showed a better compromise between the heat transfer and pressure drop values as opposed to the other angles of the ribs.

5. For the case of ribs with an angle of 60° the flow is more effectively engaged with the turbulent structures. This is due to the fact that the ribs selected are geometrical in nature as they enable the formation of secondary vortices that are small-scaled enabling them to penetrate deeper into the boundary layer enhancing the overall heat transfer rates. The boosting of the interaction between the turbulent flow and the rib surfaces results in increased convection heat transfer and therefore high Nusselt number.

6. From the study it can be concluded that at Reynolds number of 3900, the Nusselt number for 60° rib is 92.7%. The enhancement factor of the rough duct was realized to be higher than that of the smooth duct, which implies improvement in heat transfer effectiveness.

7. From the data of figures presented in result section, it is detected that the Nusselt number for 60° is approximately equal to 186.5% at Reynolds number 18500. Achieving a pressure drop more than that of the smooth duct which implies that the designed duct has enhanced ability to flow high amount of air.

8. For turbulent flow employed in this research over the 90° ribs the Nusselt number is about 143.6% at Reynolds number 5500. It is higher than that of the smooth duct, which also shows the existence of enhancement but still lower than 60° ribs.

Ultimately, this study explores the impact of rib angles on the heat exchange in solar air heaters. Their results prove that modifying solar collector ribs into ones with a V rather than a plain shape can dramatically improve heat transfer efficiency, especially when the rib angle is around 60°. However, the study highlights the limitations as well by using a very simplified CFD model and some assumptions. The findings are very helpful for various reasons such as improving solar collector design and heat transfer efficiency in solar air heaters, though the validation of experimental is needed to prove the accuracy and more insights. Future investigations may be centered around the development of the solar-air-heater design through the study of extra rib angles or structures. First, experimental validation of CFD results could enlarge the credibility and the applicability of the findings.

REFERENCES

[1] Agarwal, A. (2024). Optimizing efficiency of solar double-pass air heater through fluid combination approach. E3S Web of Conferences, 547: 03026. https://doi.org/10.1051/e3sconf/202454703026

[2] Agarwal, A. (2024). Numerical analysis of solar collector absorber tubes with C-shaped roughness for enhanced heat transfer. E3S Web of Conferences, 547: 03019. https://doi.org/10.1051/e3sconf/202454703019

[3] Abbas, S., Zhou, J., Hassan, A., Yuan, Y., Yousuf, S., Sun, Y., Zeng, C. (2023). Economic evaluation and annual performance analysis of a novel series-coupled PV/T and solar TC with solar direct expansion heat pump system: An experimental and numerical study. Renewable Energy, 204: 400-420. https://doi.org/10.1016/j.renene.2023.01.032

[4] Özdenefe, M., Alteer, K. (2022). Theoretical And experimental investigation of V-corrugated solar air heater for space heating. Isı Bilimi ve Tekniği Dergisi, 42(2): 203-220. https://doi.org/10.47480/isibted.1194986

[5] Saini, S.K., Saini, R.P. (2008). Development of correlations for Nusselt number and friction factor for solar air heater with roughened duct having arc-shaped wire as artificial roughness. Solar Energy, 82(12): 1118-1130. https://doi.org/10.1016/j.solener.2008.05.010

[6] Saini, R.P., Verma, J. (2008). Heat transfer and friction factor correlations for a duct having dimple-shape artificial roughness for solar air heaters. Energy, 33(8): 1277-1287. https://doi.org/10.1016/j.energy.2008.02.017

[7] Singh, A.P., Kumar, A., Singh, O.P. (2020). Efficient design of curved solar air heater integrated with semi-down turbulators. International Journal of Thermal Sciences, 152: 106304. https://doi.org/10.1016/j.ijthermalsci.2020.106304

[8] Thianpong, C., Chompookham, T., Skullong, S., Promvonge, P. (2009). Thermal characterization of turbulent flow in a channel with isosceles triangular ribs. International Communications in Heat and Mass Transfer, 36(7): 712-717. https://doi.org/10.1016/j.icheatmasstransfer.2009.03.027

[9] Kazemi Moghadam, H., Mousavi Ajarostaghi, S.S., Poncet, S. (2021). Numerical modeling of an innovative arc shape rib based solar air heater. Proceedings of the Institution of Mechanical Engineers, Part C: Journal of Mechanical Engineering Science, 235(24): 7992-8012. https://doi.org/10.1177/09544062211039541

[10] Kumar, A., Bhagoria, J.L., Sarviya, R.M. (2009). Heat transfer and friction correlations for artificially roughened solar air heater duct with discrete W-shaped ribs. Energy Conversion and Management, 50(8): 2106-2117. https://doi.org/10.1016/j.enconman.2009.01.025

[11] Chompookham, T., Thianpong, C., Kwankaomeng, S., Promvonge, P. (2010). Heat transfer augmentation in a wedge-ribbed channel using winglet vortex generators. International Communications in Heat and Mass Transfer, 37(2): 163-169. https://doi.org/10.1016/j.icheatmasstransfer.2009.09.012

[12] Farhan, A.A. (2017). Theoretical and experimental studies for a double pass solar air heater. International Journal of Computer Applications, 161(2): 21-26. https://doi.org/10.5120/ijca2017913117

[13] Momin, A.M.E., Saini, J.S., Solanki, S.C. (2002). Heat transfer and friction in solar air heater duct with V-shaped rib roughness on absorber plate. International Journal of Heat and Mass Transfer, 45(16): 3383-3396. https://doi.org/10.1016/S0017-9310(02)00046-7

[14] Matheswaran, M.M., Arjunan, T.V., Somasundaram, D. (2019). Energetic, exergetic, and enviro-economic analysis of parallel pass jet plate solar air heater with artificial roughness. Journal of Thermal Analysis and Calorimetry, 136: 5-19. https://doi.org/10.1007/s10973-018-7727-4

[15] Matheswaran, M.M., Arjunan, T.V., Somasundaram, D. (2018). Analytical investigation of solar air heater with jet impingement using energy and exergy analysis. Solar Energy, 161: 25-37. https://doi.org/10.1016/j.solener.2017.12.036

[16] Panda, S., Kumar, R. (2022). A review on heat transfer enhancement of solar air heater using various artificial roughed geometries. Journal of Advanced Research in Fluid Mechanics and Thermal Sciences, 89(1): 92-133. https://doi.org/10.37934/arfmts.89.1.92133

[17] Saxena, R., Pachorkar, P., Jain, A., Majumder, H., Pandey, K.K., Mishra, S.K., Kalbande, V.P. (2023). Performance enhancement of solar air heater using artificial roughness. Materials Today: Proceedings. https://doi.org/10.1016/j.matpr.2023.05.012

[18] Kumar, R., Verma, S.K., Gupta, N.K., Mendiburu, A.Z., Sharma, A., Alam, T., Eldin, S.M. (2023). Experimental assessment and modeling of solar air heater with V-shape roughness on absorber plate. Case Studies in Thermal Engineering, 43: 102784. https://doi.org/10.1016/j.csite.2023.102784

[19] Esmaeili Shayan, M., Ghasemzadeh, F., Rouhani, S.H. (2023). Energy storage concentrates on solar air heaters with artificial S-shaped irregularity on the absorber plate. Journal of Energy Storage, 74, 109289. https://doi.org/10.1016/j.est.2023.109289

[20] Hussein, N.F., Ahmed, S.T., Ekaid, A.L. (2022). Effect of tubular solar absorber on the performance of counterflow double pass solar air heater: Experimental and numerical studies. International Journal of Engineering, 35(10): 2007-2017. https://doi.org/10.5829/IJE.2022.35.10A.18

[21] Letsatsi, M.T., Agarwal, A. (2023). Investigation of concrete chimney structure using edge treatment technique based on CFD static structural analysis. In Emerging Trends in Mechanical and Industrial Engineering: Select Proceedings of ICETMIE 2022, pp. 99-111. https://doi.org/10.1007/978-981-19-6945-4_8

NOMENCLATURE

ρ	Density
v	Velocity vector
p	Pressure
τ	Stress tensor
k	Thermal conductivity/Turbulence kinetic energy
ϵ	Turbulence dissipation rate
THPF	Thermo-Hydraulic Performance Factor